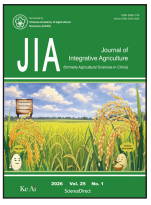
Journal of Integrative Agriculture 2026, 25(1): 42–55

Available online at ScienceDirect

Journal of Integrative Agriculture



RESEARCH ARTICLE

ZmCals12 impacts maize growth and development by regulating symplastic transport

Ziwen Shi, Sheng Zhang, Qing He, Xiaoyuan Wang, Bo Yang, Tao Yu, Hongyang Yi, Tingzhao Rong, Moju Cao[#]

State Key Laboratory of Crop Gene Exploration and Utilization in Southwest China/Maize Research Institute, Sichuan Agricultural University, Chengdu 611130, China

Highlights

- *ZmCals12* is mainly expressed in the vascular transport system, regulating callose deposition and symplastic transport.
- *ZmCals12* regulates maize growth and development by affecting sugar transport.

Abstract

Carbohydrate partitioning from source to sink tissues is essential for plant growth and development. However, in maize (*Zea mays* L.), the molecular mechanisms by which callose synthase genes regulate this process remain largely unexplored. This study demonstrates that mutation of maize *callose synthase12* (*ZmCals12*) results in increased carbohydrate accumulation in photosynthetic leaves but decreased carbohydrate content in sink tissues, leading to plant dwarfing and male sterility. Histochemical β-glucuronidase (GUS) activity assay and mRNA *in situ* hybridization (ISH) revealed that *ZmCals12* expression mainly occurs in the vascular transport system. ZmCals12 loss-of-function decreased callose synthase activity and callose deposition in plasmodesmatas (PDs) and surrounding phloem cells (PCs) of the vascular bundle. The drop-and-see (DANS) assay indicated reduced PD permeability in photosynthetic cells and diminished transport competence of leaf veins in *Zmcals12* mutants, resulting in decreased symplastic transport. Paraffin section analysis revealed that less-developed vascular cells (VCs) in *Zmcals12* mutants likely disrupted sugar transport, contributing to the pleiotropic phenotype. Furthermore, impaired sugar transport inhibited internode development by suppressing auxin (IAA) biosynthesis and signaling in *Zmcals12* mutant. These findings elucidate the mechanism by which ZmCals12-mediated callose deposition and symplastic transport regulate maize growth and development.

Keywords: maize, ZmCals12, plasmodesmata (PD) permeability, symplastic transport, less-developed vascular cells (VCs), auxin (IAA) biosynthesis and signaling

1. Introduction

Carbohydrate partitioning, the transport of carbohydrates from photosynthetic to non-photosynthetic tissues, is essential for plant growth and development (Lalonde *et al.* 2003; Braun *et al.* 2014; Yadav *et al.* 2015; Julius *et al.* 2017). The efficiency of this process significantly influences crop yield, and enhanced yields can be achieved through the manipulation of related genes (Wang *et al.* 2021). Thus, understanding carbohydrate partitioning and analyzing its molecular regulatory mechanisms holds substantial theoretical and practical significance.

In maize (*Zea mays* L.), sucrose serves as the primary carbohydrate transported to various sink tissues through the phloem (Julius *et al.* 2017). The phloem consists of three main cell types: phloem parenchyma (PP) cells, companion cells (CCs), and sieve elements (SEs). The SEs lack nuclei and rely on adjacent CCs for metabolic support, with these two cell types functioning together as the CC–SE complex (Esau 1977; van Bel and Knoblauch 2000). Sucrose synthesis occurs in mesophyll (M) cells before moving through plasmodesmata (PD) to bundle sheath (BS) cells and vascular parenchyma (VP) cells (Evert 1978;

Received 30 December 2023; Received in revised form 15 March 2024; Accepted 1 April 2024; Available online 13 May 2024
Ziwen Shi, E-mail: ziwen_shi@163.com; [#]Correspondence Moju Cao, Tel: +86-28-86290916, E-mail: caomj@sicau.edu.cn

© 2026 CAAS. Publishing services by Elsevier B.V. on behalf of KeAi Communications Co. Ltd. This is an open access article under the CC BY-NC-ND license (http://creativecommons.org/licenses/by-nc-nd/4.0/). Peer review under responsibility of Editorial Board of *Journal of Integrative Agriculture*.
doi: 10.1016/j.jia.2024.05.010

Braun and Slewinski 2009). In maize, PD is rare at the interface of the BS or PP cells and CC-SE complex (Evert *et al.* 1978). Consequently, sucrose exits the BS or PP cells into the phloem apoplast *via* SUGARS WILL EVENTUALLY BE EXPORTED TRANSPORTER (SWEET) proteins and enters the CC–SE complex through the SUCROSE TRANSPORTER1 (SUT1) protein (Braun and Slewinski 2009; Eom *et al.* 2015; Baker *et al.* 2016; Bezrutczyk *et al.* 2018, 2021). Subsequently, sucrose moves from CCs to SEs through PDs, with the SEs forming sieve tubes through end-to-end connections *via* porous sieve plates (SPs), enabling long-distance transport to sink tissues (Esau 1977; Evert 1982).

Callose, a β-(1,3)-glucan polymer with 1,6 branches, exists at minimal levels primarily in pollen mother cells, PDs, cell walls, and cell plate regions. This compound plays essential roles in cell wall formation during growth, cell plate formation during cytokinesis, PD function, and sieve pore development during vascular differentiation. Additionally, it contributes to pollen development, sugar transport, and responses to abiotic and biological stress (Verma and Hong 2001; Slewinski *et al.* 2012; Cui and Lee 2016; Shi *et al.* 2016; Amsbury *et al.* 2017; Wu *et al.* 2018; Liu *et al.* 2022). Symplastic transport is mediated by PDs (Zambryski and Crawford 2000; Roberts and Oparka 2003). PD permeability is the key factor that determines the symplast transport, and is controlled by the deposition and degradation of callose (Han *et al.* 2014; Kitagawa and Jackson 2017; Wu *et al.* 2018). In *Arabidopsis*, the *cals3m* mutant exhibited increased callose deposition at PD neck regions in roots, leading to decreased PD permeability and reduced phloem unloading from CCs to the endodermis (Vatén *et al.* 2011). *AtCalS7* regulates SP development and sugar transport; its loss of function results in reduced callose deposition in SE and smaller and fewer sieve pores, impeding sucrose transport (Barratt *et al.* 2011; Xie *et al.* 2011). In rice, both the *osgsl5* mutant, a *Glucan Synthase-Like 5* (*GSL5*) knock-out mutant, and the *cannot reach the roof 1* (*crr1*) mutant, two glucan synthase-like mutants, exhibited impaired ovary expansion and anther development. The *crr1* mutant showed decreased callose deposition in PDs and vascular tissue developmental defects, likely inhibiting sugar transport to reproductive organs (Shi *et al.* 2015; Song *et al.* 2016). In maize, the *tie-dyed1* (*tdy1*), *tdy2* and *Carbohydrate partitioning defective1* (*Cpd1*) mutants affect carbohydrate partitioning due to abnormal callose deposition at PDs or SPs (Baker and Braun 2007, 2008; Ma *et al.* 2008; Slewinski *et al.* 2008, 2012; Baker *et al.* 2013; Julius *et al.* 2018). These studies suggest that reduced, enhanced or ectopic callose deposition in PDs and/or SPs can affect carbohydrate phloem loading, unloading, and partitioning to sink tissues.

To date, at least 12 maize mutants with abnormal carbohydrate partitioning have been reported. These mutants can be roughly classified into four groups: (1) Five mutants with impaired symplastic transport mediated by PDs, including *sucrose export defective1* (*sxd1*), *tdy1*, *tdy2*, *Cpd1* and *cpd33*. *SXD1*, encoding a tocopherol cyclase, participates in vitamin E biosynthesis. The *sxd1* mutant exhibited ectopic callose deposition in PDs between BS and VP cells, hindering sucrose symplastic transport (Russin *et al.* 1996; Botha *et al.* 2000; Provencher *et al.* 2001). *TDY2*, encoding a callose synthase, demonstrates high expression in the vascular tissue of developing leaves. The mutation of *TDY2* decreased sucrose symplastic transport from CCs into SEs (Slewinski *et al.* 2012). *TDY1*, encoding a novel and function-unknown transmembrane protein, functions in the same pathway as *TDY2* (Baker and Braun 2008; Ma *et al.* 2008, 2009; Slewinski *et al.* 2008; Baker *et al.* 2013). *Cpd1*, a semi-dominant mutant, displays ectopic callose deposits in SEs, likely inhibiting sucrose symplastic transport in SPs (Julius *et al.* 2018). *CPD33*, encoding a multiple C2 domains and transmembrane region protein (MCTP), may regulate sucrose transport rates by influencing PD formation at the CC-SE interface (Tran *et al.* 2019). (2) Three mutants with impaired apoplastic transport mediated by SWEETs and SUTs, including *sugars will eventually be exported transporter13a;b;c* (*sweet13a;b;c*), *sweet4c*, *sucrose transporter1* (*sut1*), *sucrose transporter2* (*sut2*), and *sucrose and glucose carrier 1* (*sugcar1*). ZmSWEET13a, b and c localize to the PP plasma membrane and transport sucrose from the PP into the apoplasm. The *zmsweet13a;b;c* mutant showed excessive carbohydrate accumulation in leaves and severe growth retardation (Bezrutczyk *et al.* 2018, 2021). *ZmSWEET4c* mediates transepithelial hexose transport across the basal endosperm transfer layer (BETL) and the entry point of nutrients into the seed. The mutation of *ZmSWEET4c* impaired further transfer of sugars imported from the maternal phloem, resulting in seed filling defects (Sosso *et al.* 2015). SUT1 is localized to the CC plasma membrane and transports sucrose from the apoplasm into the CC. The *sut1* mutant exhibited excessive carbohydrate accumulation in leaves and inhibited growth of sink tissues (Slewinski *et al.* 2009, 2010; Baker *et al.* 2016). SUT2, localized to the tonoplast, participates in sucrose remobilization from vacuoles for growing tissues (Leach *et al.* 2017). *ZmSUGCAR1* mediates sucrose and glucose transport and is specifically expressed in the BETL. Its loss-of-function mutation caused significantly decreased sucrose and glucose contents and subsequent shrinkage of maize kernels (Yang *et al.* 2022). (3) Two mutants with impaired vasculature development, including *Cpd1*, the *cpd28* and *cpd47* mutants of *Brittle Stalk2-Like3* (*Bk2L3*). *CPD1* and *Bk2L3* influence vasculature system structure formation (Julius *et al.* 2018). *Bk2L3* encodes a COBRA-like protein involved in cell wall development. The *cpd28* and *cpd47* mutants exhibited reduced cellulose accumulation in leaves, leading to abnormal SE cell wall ultrastructure and hindered carbohydrate partitioning (Julius *et al.* 2021). (4) One mutant with impaired transitory starch remobilization is *chlorotic leaf3* (*chl3*). *CHL3* encodes starch phosphorylase 2. The *chl3* mutant showed hindered transitory starch remobilization at night and excessive carbohydrate accumulation in leaves, inhibiting chloroplast development and photosynthetic gene expression (Qin *et al.* 2022). These mutants generally exhibit chlorotic leaves, reduced plant height, and decreased fertility, associated with inhibited carbohydrate partitioning.

Our previous study demonstrated that the *ms39* mutant, which exhibited plant dwarfing and male sterility,

was controlled by a recessive nuclear gene (Zhu *et al.* 2018). Subsequently, we confirmed that a mutation in *Zm00001d043909* (*ZmCals12*), encoding a callose synthase, is responsible for the male sterility of the *ms39* mutant (Niu *et al.* 2023). In this study, we investigated the role of *ZmCals12* in symplastic transport. The results reveal that *ZmCals12* is involved in regulating callose deposition in PDs and around phloem cells (PCs) of the vascular bundle, as well as the number of vascular cells (VCs), which influences sugar transport and maize growth and development.

2. Materials and methods

2.1. Plant materials and growth environment

Maize (*Zea mays* L.) inbred lines Mo17, KN5585, the introgression line of *ms39* in the Mo17 background (Mo17^{ms39}) derived from (*ms39*×Mo17) BC_8F_2 population, and two editing lines, *MS39*KO#2 and *MS39*KO#3 lines, previously designated as *Cr-MS39-2* and *Cr-MS39-3* lines (Niu *et al.* 2023), were cultivated in the experimental field in Sichuan Province (30.97°N, 103.82°E), China.

2.2. Morphology and cytological analyses

The 12-wk-old Mo17, Mo17^{ms39}, KN5585, *MS39*KO#2, and *MS39*KO#3 plants were analyzed for internode number and length measurements. The ear internode was designated as 0 internode, with internodes above the ear internode successively labeled as +1 internode, +2 internode, and internodes below the ear internode labeled as –1 internode, –2 internode, continuing until all internodes were numbered.

The ear internode of 12-wk-old Mo17, Mo17^{ms39}, KN5585, *MS39*KO#2, and *MS39*KO#3 plants were examined for internode cell number and length measurements. Five mature leaves of 5-wk-old Mo17, Mo17^{ms39}, KN5585 and *MS39*KO#2 plants were analyzed for lateral and minor vein counts, with six lateral veins near the leaf center of each mature leaf measured for lateral vein area, VC number and area. Five +1, 0 and –1 internodes of 12-wk-old Mo17 and Mo17^{ms39} plants were analyzed for vascular bundle count and cross-sectional area, with six vascular bundles near the internode center of each internode measured for vascular bundle area. Paraffin sectioning was performed as described (Bezrutczyk *et al.* 2021). Sections (4 μm) were cut and stained with filtered 0.1% toluidine blue. Microscopic images were obtained using a Zeiss Axio Imager M2 microscope (Zeiss, Germany). Section length and area were measured using ZEN 2.3 (blue edition) software (Zeiss). For aniline blue staining, longitudinal sections were stained with 0.1% aniline blue and visualized under ultraviolet (UV) illumination using a Zeiss Axio Imager M2 microscope (Zeiss). Callose fluorescence of SPs was quantified using ZEN 2.3 (blue edition) software (Zeiss).

2.3. Starch staining

Starch staining was performed as previously described (Baker and Braun 2007). Briefly, mature leaves from 5-wk-old Mo17, Mo17^{ms39}, KN5585, *MS39*KO#2, and *MS39*KO#3 plants were collected at 5:00 a.m. and 5:00 p.m., and boiled in 95% ethanol for 30 min. Samples were then stained with 1.25% (iodine-potassium iodide) I_2-KI for 5 min. Subsequently, free-hand section was performed and imaged using a Zeiss Axio Imager M2 microscope (Zeiss).

2.4. Soluble sugar and starch measurements

Mature leaves from 5-wk-old Mo17 and Mo17^{ms39} plants were harvested at 5:00 a.m. Starch and soluble sugars were extracted as previously described (Leach and Braun 2016). The extracts were analyzed using high-performance anion-exchange chromatography (ICS-5000, Thermo Fisher Scientific, USA) according to previously established methods (Leach *et al.* 2017).

Leaves, internodes, tassels, ears, and roots were collected from 10-wk-old Mo17 and Mo17^{ms39} plants at 5:00 p.m. The contents of total starch, sucrose, glucose, and fructose were determined separately using assay kits BC0705, BC2465, BC2505 and BC2455 (Solarbio, China) following the manufacturer's protocols.

2.5. Transmission electron microscopy (TEM)

Mature leaves from 5-wk-old Mo17 and Mo17^{ms39} plants were collected at 5:00 a.m. The pre-fixation solution consisted of 2.5% (w/v) glutaraldehyde in 100 μmol L^{-1} phosphate buffer (pH 7.4), while the fixation solution contained 1% (w/v) OsO_4 in the same buffer. Samples were then dehydrated using a graded ethanol series before embedding in epoxy resin (SPI-PON 812, SPI Supplies; Structure Probe Inc., PA, USA). Ultrathin sections were prepared using a Leica EM UC7 ultramicrotome (Leica, Germany) and stained sequentially with uranyl and lead citrate. Images were captured using a JEM-1400FLASH transmission electron microscope (JEOL, Japan).

2.6. Auxin (IAA) biosynthesis components quantification

IAA biosynthesis components were extracted from stems of 10-wk-old Mo17 and Mo17^{ms39} plants (including +1 and +2 internodes) and analyzed using ultrafast liquid chromatography with electrospray ionization and tandem mass spectrometry (UFLC-ESI-MS, Shimadzu, Japan; Applied Biosystems, USA) as previously described (Liu *et al.* 2012).

2.7. RNA isolation and RT-qPCR

Total RNA was extracted using 1 mL of RNAiso Plus reagent (TaKaRa, Japan) according to the manufacturer's instructions. For reverse transcription, 1 μg of total RNA was used and first-strand cDNA was synthesized using HiScript III RT SuperMix for qPCR (+gDNA wiper) (Vazyme, China) following the manufacturer's protocol. RT-qPCR was performed with TB Green® *Premix Ex Taq*™ (Tli RNaseH Plus) (TaKaRa, Japan) using a Bio-Rad CFX96 Touch Real-Time PCR Detection System (Bio-Rad, USA). *ZmActin* was used as an internal control (Chen *et al.* 2017). The analysis included three biological replicates. Relative expression was calculated using the $2^{-\Delta\Delta Ct}$ method (Livak and Schmittgen 2001).

2.8. Histochemical β-glucuronidase (GUS) activity assay

The 1.8 kb promoter of *ZmCals12* and the enhanced green fluorescent protein (eGFP) were amplified from Mo17 and

pCAMBIA2300, respectively, then cloned into pCAMBIA3301. The resulting vector ZmCals12pro::eGFP-GUS was transformed into KN5585. Histochemical GUS activity assay was performed as previously described (Bezrutczyk *et al.* 2021). The X-Gluc-stained tissue was observed using a Leica M205FA microscope (Leica, Germany). For paraffin sections, the X-Gluc-stained tissue was fixed in FAA solution, and then embedded in paraplast. 10-μm sections were cut using a Leica RM2255 microtome (Leica). Sectioned samples were observed using a Zeiss Axio Imager M2 microscope (Zeiss).

2.9. mRNA *in situ* hybridization (ISH)

mRNA ISH was performed according to previously described methods (Bezrutczyk *et al.* 2021). The sense and antisense probes of *MS39* were labelled using digoxigenin. Mature leaves from 5-wk-old plants and elongating internodes from 10-wk-old Mo17 plants were collected, fixed, dehydrated, sliced, pre-hybridized, and hybridized. Samples were then incubated with anti-DIG AP-conjugated antibody and nitro blue tetrazolium chloride (NBT)/5-bromo-4-chloro-3-indolyl-phosphate (BCIP), followed by washing and sealing. Finally, samples were observed using a PANNORAMIC SCAN II (3DHISTECH, Hungary).

2.10. Callose immunofluorescence localization

Callose immunofluorescence localization was performed as previously described (Wang *et al.* 2022). In brief, mature leaves from 5-wk-old Mo17, Mo17^{ms39}, KN5585, *MS39*KO#2 and *MS39*KO#3 plants were fixed in 4% paraformaldehyde for 24 h at room temperature, embedded in agar blocks and cut with a vibrating slicer (Leica). The samples were blocked with phosphate buffered saline (PBS) solution containing 0.5% skim milk and 0.2% bovine serum albumin (BSA), then washed and incubated with anti-callose antibody (Cat. No. 400-2, Biosupplies, Yagoona, Australia) at 1:200 dilution in PBS solution overnight at 4°C. After PBS washing, anti-mouse FITC (Invitrogen, USA) diluted 1:400 in PBS solution was applied for 5 h at room temperature, followed by PBS washing. GFP and UV signals were detected using a PANNORAMIC SCAN II (3DHISTECH, Hungary). Samples without antibody addition served as negative controls.

2.11. Callose quantification

Callose quantification was performed according to previously established methods (Wang *et al.* 2022). Callose was extracted from mature leaves of 5-wk-old Mo17, Mo17^{ms39}, KN5585, *MS39*KO#2, and *MS39*KO#3 plants and quantified through fluorescence spectrophotometry using laminarin (LE, kelp polysaccharide) as the standard. The excitation wavelength was set at 405 nm, and the emission wavelength was set at 500 nm.

2.12. Callose synthase activity measurement

Callose synthase activity measurement followed previously established protocols (Wang *et al.* 2022). Briefly, mature leaves from 5-wk-old Mo17, Mo17^{ms39}, KN5585, *MS39*KO#2, and *MS39*KO#3 plants were collected for total protein extraction. Protein concentration was measured using an assay kit P0006C (Beyotime, China) according to manufacturer's instructions. For enzymatic reaction, 20 μL total protein containing callose synthase and 70 μL reaction solution (50 mmol L^{-1} Tris/HCl, pH 7.3, 0.02% digitonin, 2 mmol L^{-1} $CaCl_2$, 20 mmol L^{-1} cellobiose, 0.5 mmol L^{-1} UDP-GLC) were added to 1.5 mL centrifuge tube and reacted at room temperature for 1 h. Then, 10 μL of 10 mol L^{-1} NaOH was added to terminate the reaction, and the reaction system was oscillated and incubated at 80°C for 30 min to dissolve the callose. Callose content determination followed the callose quantification method.

2.13. The drop-and-see (DANS) assay

The DANS assay was conducted on leaves from 3-wk-old Mo17, Mo17^{ms39}, KN5585, *MS39*KO#2, and *MS39*KO#3 plants following established protocols (Tran *et al.* 2019). In brief, the adaxial surface of leaf was gently abraded with fine-grain sandpaper (2,000 grain) to remove the cuticle. A 1 μL solution of carboxyfluorescein succinimidyl amino ester (CFSE) (Thermo Fisher Scientific, America) (50 mg mL^{-1}) was loaded on the adaxial surface of the abraded region. After 3 min, leaf segments were cut and carboxyfluorescein (CF) signals were observed using a Zeiss Axio Imager M2 microscope (Zeiss) with standard GFP settings of 450–490 nm excitation and 500–550 nm detection range. PD permeability was represented by the ratio of fluorescent signal intensity on the abaxial surface to that on the adaxial surface, as described (Tran *et al.* 2019). To examine leaf vein transport competence, 1 μL of CFSE solution (50 mg mL^{-1}) was applied to the leaf through gentle abrasion of the adaxial epidermal surface. After 5 min, leaf segments were cut and CF signals in leaf veins were observed using a Zeiss Axio Imager M2 microscope (Zeiss) with standard GFP settings.

3. Results

3.1. *ZmCals12* is mainly expressed in the vascular transport system

To identify the expression pattern of *ZmCals12*, we performed a histochemical GUS activity assay using transgenic plants harboring a ZmCals12pro::eGFP-GUS reporter construct, where the eGFP and GUS reporter genes were placed under the control of the *MS39* (*ZmCals12*) promoter (Appendix A). Histochemical analysis revealed strong GUS signals in the vascular tissues of leaf and leaf sheath, the junction of leaf-leaf sheath and leaf sheath-stem, node, ear primordium, and tassel (Fig. 1-A). Detailed observations for tassel demonstrated the localization of strong GUS signal in central spike, junctions of central spike-branch, central spike/branch-pedicellate spikelet, central spike/branch-sessile spikelet, spikelet glumes, and rachilla (Fig. 1-A). mRNA ISH also showed that *MS39* was expressed in vascular bundle of leaf but not internode (Fig. 1-B). These results demonstrate that *ZmCals12* is mainly expressed in the vascular transport system. Additionally, RT-qPCR analysis of *ZmCals12* expression in leaves and leaf sheaths of 5-wk-old Mo17, Mo17^{ms39}, KN5585, *MS39*KO#2, and *MS39*KO#3 indicated reduced transcription levels in *Zmcals12* mutants (Appendix B).

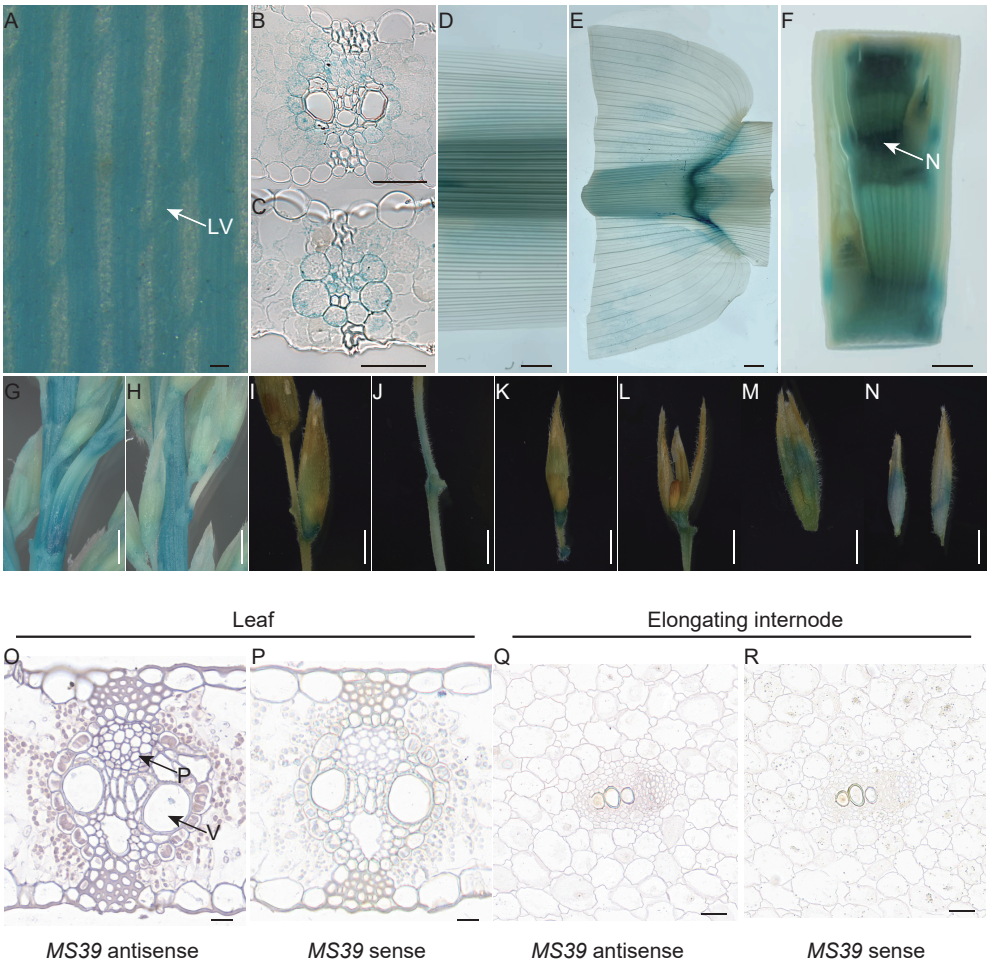


Fig. 1 Analysis of the tissue-specific expression of *ZmCals12*. A, β-glucuronidase (GUS) staining in leaf of ZmCals12pro::eGFP-GUS plant. LV, leaf vein. The transverse sections of lateral vein (B) and minor vein (C) from A, respectively. Scale bars=50 μm (A–C). D–F, GUS staining in leaf sheath (D), leaf-leaf sheath and stem (E) and stem (F). N, node. Scale bars=0.5 cm. G–N, GUS staining in central spike-branch and central spike-pedicellate/sessile spikelet (G and H), branch-sessile spikelet (I), branch (J), pedicellate spikelet (K), pedicellate spikelet (L), outer glume (M), and inner glume (N) of ZmCals12pro::eGFP-GUS plant. Scale bars=2 mm. O–R, detection of *MS39* mRNA accumulation pattern by mRNA *in situ* hybridization (ISH) in transverse sections of 5-wk-old mature leaf (O and P) and 10-wk-old elongating internode (Q and R). No staining was observed following hybridization with *MS39* sense probe (negative control) (P and R). V, xylem vessel; P, phloem. Scale bars=20 μm.

3.2. ZmCals12 is involved in callose deposition in PDs and around PCs of vascular bundle

The abnormal deposition of callose in PDs and/or SPs can affect carbohydrate phloem loading, phloem unloading, or transport to sink tissues by regulating symplastic transport (Shi *et al*. 2015; Song *et al*. 2016; Julius *et al*. 2018). To explore whether *ZmCals12* affects callose deposition in PDs, callose immunofluorescence localization was performed to determine the callose deposition in mature leaves from 5-wk-old Mo17, Mo17^{ms39}, KN5585, *MS39*KO#2, and *MS39*KO#3 plants. The analysis revealed obviously reduced callose deposition in PDs and around PCs of vascular bundle in Mo17^{ms39}, *MS39*KO#2 and *MS39*KO#3 leaves compared to Mo17 and KN5585, respectively (Fig. 2-A–E; Appendix C). Callose quantification confirmed significantly lower callose content in Mo17^{ms39}, *MS39*KO#2 and *MS39*KO#3 mature leaves compared to Mo17 and KN5585, respectively (Fig. 2-F and G). Furthermore, aniline blue staining analysis showed no significant difference in callose deposition at SPs of the mature leaves of 5-wk-old Mo17 and Mo17^{ms39} (Appendix C).

To further explore whether the reduced callose deposition correlates with ZmCals12 catalytic activity, callose synthase activity was measured in mature leaves from 5-wk-old Mo17, Mo17^{ms39}, KN5585, *MS39*KO#2, and *MS39*KO#3 plants. The results indicated significantly reduced callose synthase activity in Mo17^{ms39}, *MS39*KO#2 and *MS39*KO#3 leaves compared to Mo17 and KN5585, respectively (Fig. 2-H and I). Collectively, these results indicate that ZmCals12 is involved in regulating callose deposition in PDs and around PCs of vascular bundle.

3.3. ZmCals12 regulates symplastic transport by affecting PD permeability

To investigate whether the reduced callose deposition affects PD permeability, DANS assays were performed with the adaxial-abaxial leaf axis of Mo17, Mo17^{ms39}, KN5585, *MS39*KO#2 and *MS39*KO#3 (Tran *et al*. 2019). The results

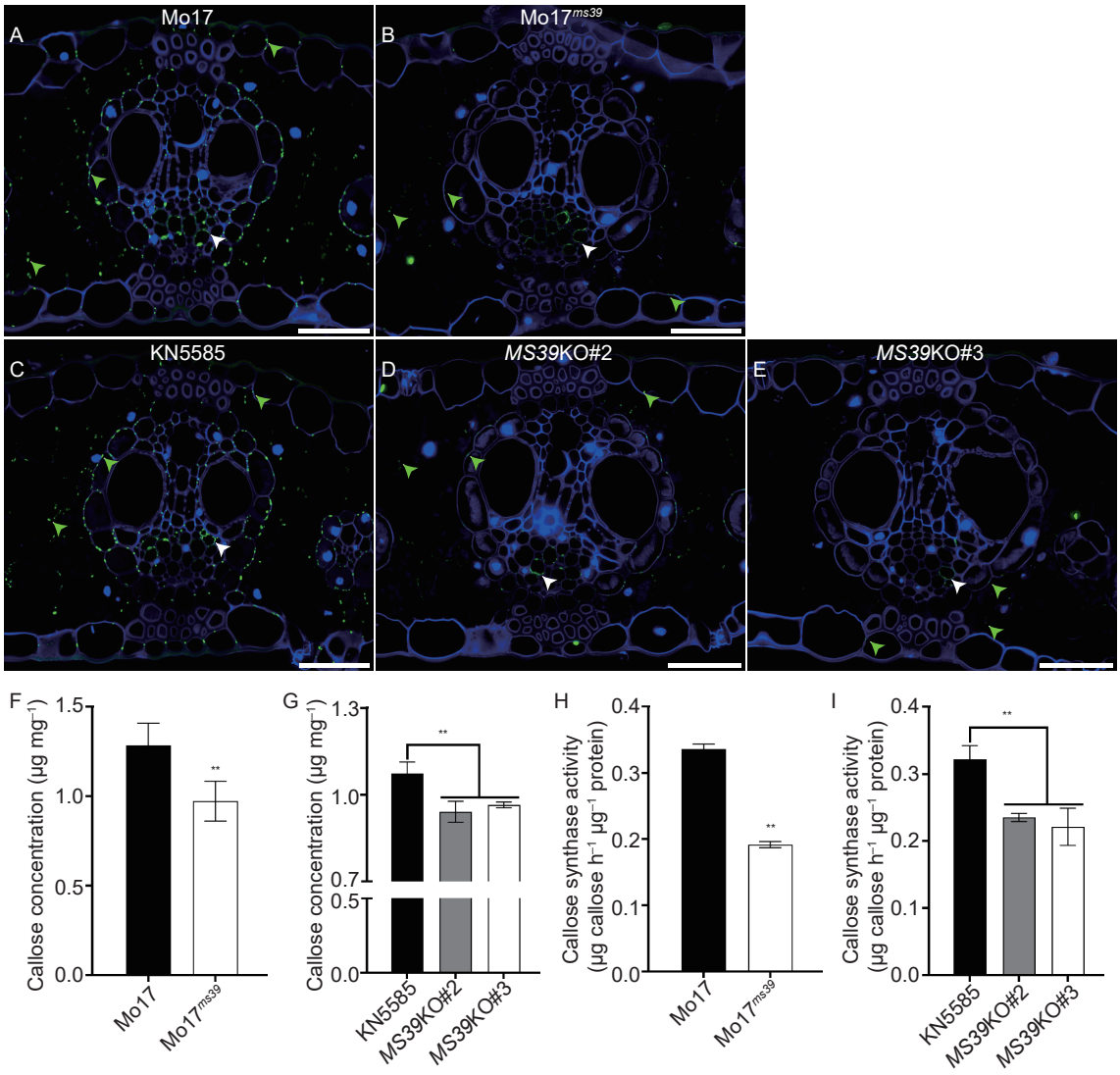


Fig. 2 Callose quantification, callose synthase activity measurement and callose immunofluorescence localization. Callose immunofluorescence localization in mature leaves of 5-wk-old Mo17 (A), Mo17^{ms39} (B), KN5585 (C), *MS39*KO#2 (D) and *MS39*KO#3 (E). The green arrows indicate callose distribution in plasmodesmatas (PDs), while the white arrows indicate callose distribution around the phloem cells (PCs) of the vascular bundle. The green fluorescence signals represent the spontaneous fluorescence of the cell wall and callose accumulation detected by antibodies, whereas the blue fluorescence signals represent spontaneous fluorescence of the cell wall. Scale bars=50 μm. F and G, biochemical quantification of callose in mature leaves of 5-wk-old Mo17, Mo17^{ms39}, KN5585, *MS39*KO#2, and *MS39*KO#3. H and I, callose synthase activity measurement in mature leaves of 5-wk-old Mo17, Mo17^{ms39}, KN5585, *MS39*KO#2, and *MS39*KO#3. Data are mean±SD (n=3). Asterisks indicate significant differences determined using a two-tailed Student's t-test (**, P<0.01).

demonstrated that the CF signal intensity in abaxial surfaces of Mo17^{ms39}, *MS39*KO#2 and *MS39*KO#3 leaves was diminished compared to Mo17 and KN5585, respectively (Fig. 3-A). Quantitative analysis of the fluorescence intensity ratio between the abaxial and adaxial epidermis revealed significant reduction in Mo17^{ms39}, *MS39*KO#2 and *MS39*KO#3 leaves compared to Mo17 and KN5585, respectively (Fig. 3-B). These findings suggest that the mutation of *ZmCals12* reduces the PD permeability of photosynthetic cells. To further explore whether the decreased PD permeability affects the transport competence of leaf veins in the *Zmcals12* mutants, CF transport was observed in leaf veins of Mo17, Mo17^{ms39}, KN5585, *MS39*KO#2, and *MS39*KO#3. The transport competence of the phloem-mobile dye CF in Mo17^{ms39}, *MS39*KO#2 and *MS39*KO#3 leaf veins exhibited obvious reductions compared to Mo17 and KN5585, respectively (Fig. 4). These results indicate that the mutation of *ZmCals12* reduces the transport competence of leaf veins.

3.4. Loss-of-function of ZmCals12 reduces sugar transport from source leaves to sink tissues

To determine whether ZmCals12 influences carbohydrate phloem loading and transport to sink tissues, mature leaves were collected from 5-wk-old Mo17, Mo17^{ms39}, KN5585, *MS39*KO#2 and *MS39*KO#3 plants at 5:00 a.m. and 5:00 p.m., respectively. After removing photosynthetic pigments, starch staining was performed with I_2-KI. The results revealed that Mo17^{ms39}, *MS39*KO#2 and *MS39*KO#3 leaves stained dark brown, while Mo17 and KN5585 leaves exhibited light brown coloration, indicating enhanced starch accumulation

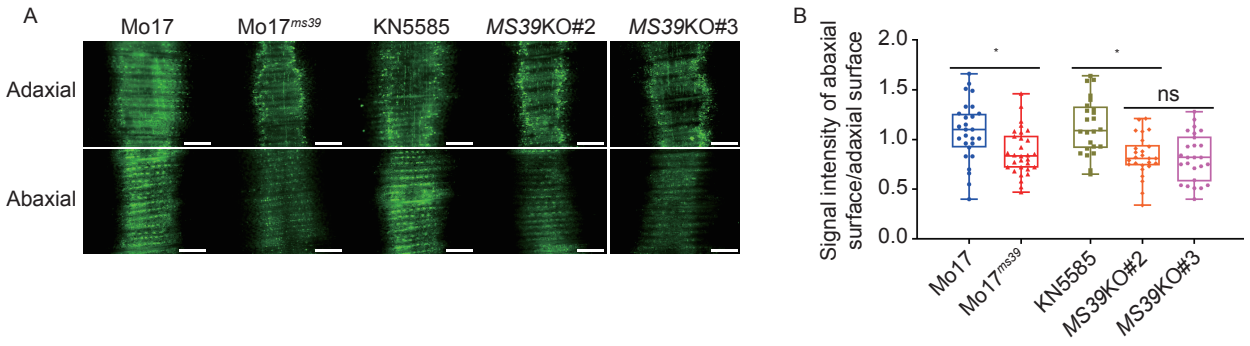


Fig. 3 Drop-and-see (DANS) assay for plasmodesmata (PD) permeability. Green fluorescence signals in A represent the carboxyfluorescein (CF) signals on the adaxial surface and abaxial surface, respectively. Signal intensity represents the PD permeability. Scale bars=500 μm. B, quantification of PD permeability with Mo17 (*n*=27), Mo17^{ms39} (*n*=30), KN5585 (*n*=24), *MS39*KO#2 (*n*=26), and *MS39*KO#3 (*n*=26) leaves. The central line, box and whiskers in boxplots indicate the median, the first and third quartiles, and the minimum and maximum values, respectively. Asterisks indicate significant differences determined using a two-tailed Student's *t*-test (*, *P*<0.05; ns, *P*>0.05).

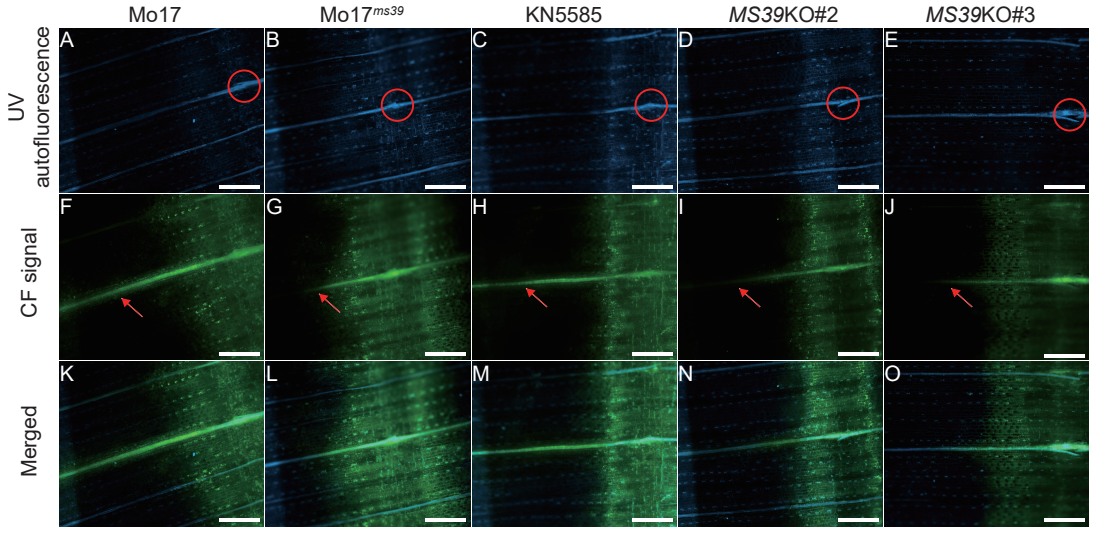


Fig. 4 Drop-and-see (DANS) assay for the transport competence of leaf veins. A–E, the ultraviolet (UV) autofluorescence. F–J, green fluorescence signals representing the carboxyfluorescein (CF) signals. CF moves in leaf veins from the leaf tip to the leaf base. K–O, merged image with UV and GFP fields. The red circles in A–E indicate sites of vein abrasion and carboxyfluorescein succinimidyl amino ester (CFSE) application, while the red arrows in F–G indicate the CF signals in leaf veins. Scale bars=500 μm.

in Mo17^{ms39}, *MS39*KO#2 and *MS39*KO#3 leaves (Fig. 5-A). Quantification of soluble sugar content in mature leaves from 5-wk-old plants collected at 5:00 a.m. showed significantly higher levels of sucrose, glucose, fructose, and maltose in Mo17^{ms39} leaves compared to Mo17 (Fig. 5-B), corroborating the starch staining results. Additionally, TEM analysis revealed that BS cells of 5-wk-old Mo17^{ms39} mature leaves contained more starch than Mo17 (Fig. 5-C).

Further, leaves, internodes, tassels, ears and roots from 10-wk-old Mo17 and Mo17^{ms39} plants were collected at 5:00 p.m., respectively, and the contents of starch, sucrose, glucose and fructose were measured in each tissue. The results showed significantly higher levels of starch, sucrose, glucose and fructose in Mo17^{ms39} leaves compared to Mo17 (Fig. 6), consistent with the carbohydrate hyperaccumulation observed in 5-wk-old Mo17^{ms39} mature leaves (Fig. 5). Notably, starch and sucrose contents in Mo17^{ms39} internodes were significantly lower than in Mo17 (Fig. 6-A and B). Similarly, starch, sucrose and fructose contents in Mo17^{ms39} tassels and ears showed significant reduction compared to Mo17 (Fig. 6-A, B and D). Collectively, these data indicate that ZmCals12 loss-of-function impairs sugar transport from source leaves to sink tissues.

3.5. ZmCals12 impacts the development of leaf vein and internode by inhibiting cell cycle progression

To explore whether reduced sugar transport correlates with abnormal vascular bundle development, we examined cross-sections of mature leaves from 5-wk-old Mo17, Mo17^{ms39}, KN5585 and *MS39*KO#2 using paraffin sectioning. The analysis revealed that while the number of vascular bundles remained similar between Mo17^{ms39} and Mo17, as well as between *MS39*KO#2 and KN5585 (Appendix D), the vascular bundle area was reduced in both Mo17^{ms39} and *MS39*KO#2 leaves compared to their respective controls, primarily due to decreased VC

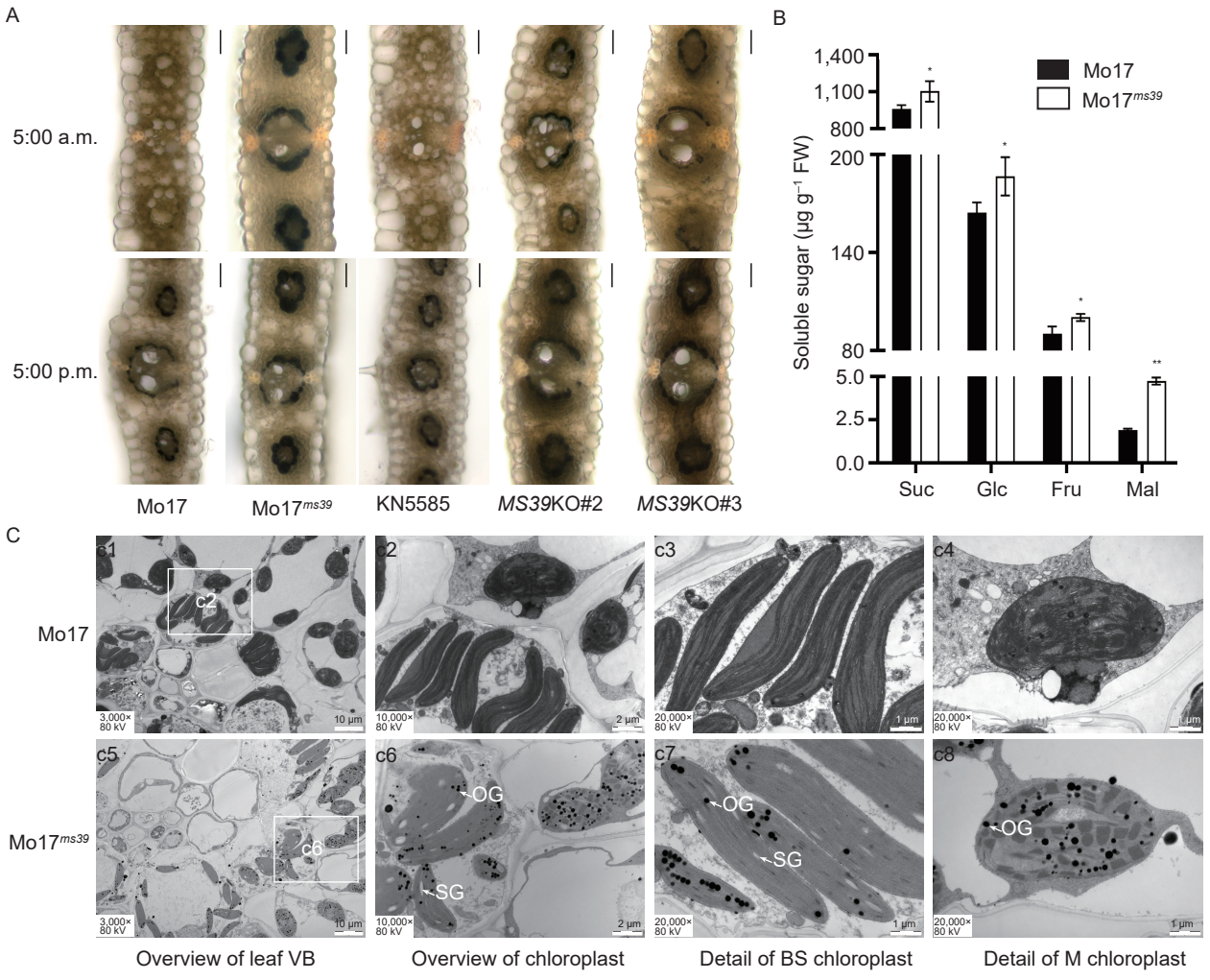


Fig. 5 Qualitative and quantitative analysis of carbohydrates in mature leaves. A, starch staining of free-hand cross-sections of Mo17 and Mo17^{ms39}, KN5585, *MS39*KO#2 and *MS39*KO#3 mature leaves collected at 5:00 a.m. and 5:00 p.m. Scale bars=40 μm. B, soluble sugar measurements in Mo17 and Mo17^{ms39} mature leaves. Suc, sucrose; Glc, glucose; Fru, fructose; Mal, maltose. Data are mean±SD (n=3). Asterisks indicate significant differences determined using a two-tailed Student's t-test (*, P<0.05; **, P<0.01). C, transmission electron microscopy (TEM) analysis of Mo17 and Mo17^{ms39} mature leaves. c1 and c5, overview of leaf vascular bundle (VB) from Mo17 and Mo17^{ms39} mature leaves. c2 and c6, overview of mesophyll (M) and bundle sheath (BS) chloroplasts from Mo17 and Mo17^{ms39} mature leaves. c3, c4, c7 and c8, detailed view of BS and M chloroplasts from Mo17 and Mo17^{ms39} mature leaves. SG, starch granule; OG, osmium globules.

numbers (Fig. 7). Additionally, examination of 12-wk-old Mo17 and Mo17^{ms39} internode cross-sections showed no significant differences in vascular bundle number, cross-sectional area, or vascular bundle area (Appendix E). These results indicate that the mutation of *ZmCals12* leads to the less-developed VCs, potentially disrupting carbohydrate transport.

The *ms39* mutant displayed male sterility and plant dwarfing (Niu *et al.* 2023). Further analysis revealed that the *Zmcals12* mutants exhibited significantly reduced internode number and length compared to Mo17 and KN5585, respectively (Appendices F and G). The reduced internode length resulted from both shortened internode cell length and decreased internode cell number (Appendix F).

To determine whether the reduced internode length and VC number in the *ms39* mutant were associated with cell division, 16 core cell cycle-related genes (CCRs), including cyclin-dependent kinases (CDKs), cyclins (CYCs) and others (Hu *et al.* 2010; Kamal *et al.* 2021), were selected and detected in 5-wk-old mature leaves and 10-wk-old stems of Mo17 and Mo17^{ms39} using RT-qPCR. The analysis demonstrated the downregulation of 15 core CCRs in Mo17^{ms39} leaf and eleven in Mo17^{ms39} stem, while the remaining genes showed no significant differences between Mo17 and Mo17^{ms39} (Fig. 8-A and B). These results suggest that abnormal leaf vein and internode development in the *ms39* mutant correlates with inhibited cell cycle progression.

3.6. Plant dwarfing of the *ms39* mutant is related to inhibited IAA biosynthesis and signaling

IAA, a simple small molecule, regulates numerous plant developmental responses through spatiotemporal control of cell division, growth, and differentiation (Zhao 2018; Gallei *et al.* 2020). Analysis of IAA biosynthesis components in stems of 10-wk-old Mo17 and Mo17^{ms39} revealed increased levels of indole-3-pyruvic acid (IPyA) and indoleacetamide (IAM), precursors of IAA biosynthesis, in Mo17^{ms39} stem compared

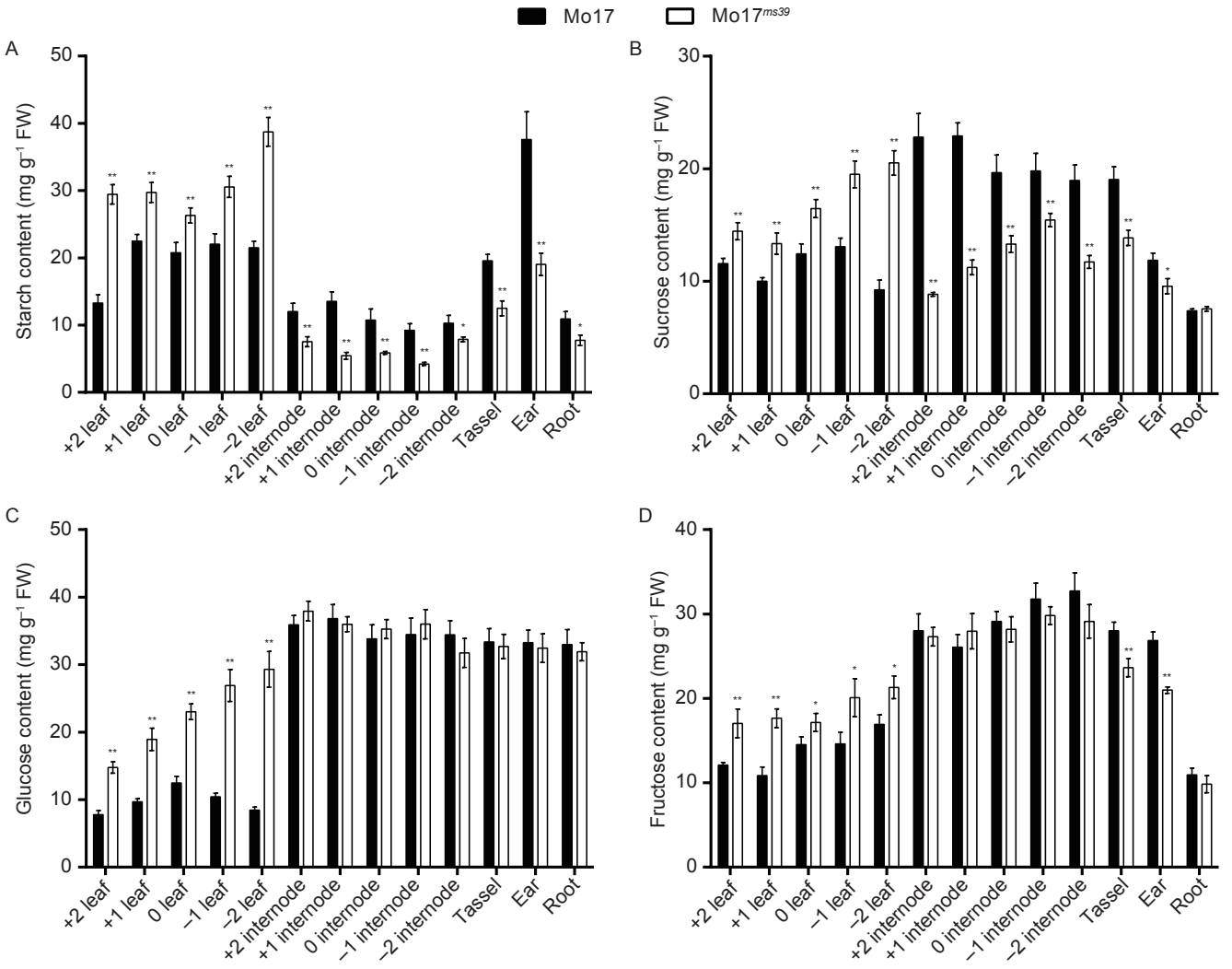


Fig. 6 Comparative analysis of starch and soluble sugar contents in various tissues between Mo17 and Mo17^{ms39}. A–D, the contents of starch, sucrose, glucose, and fructose in leaves, internodes, tassels, ears and roots collected at 5:00 p.m. Data are mean±SD (n=3). Asterisks indicate significant differences determined using a two-tailed Student's t-test (*, P<0.05; **, P<0.01).

to Mo17, while IAA content decreased (Fig. 8-C). The IPyA pathway has been established as the prevailing route for IAA synthesis in plants (Casanova-Sáez *et al*. 2021). Eight YUCCA (YUC) family genes, converting IPyA to IAA (Korasick *et al*. 2013), were selected and detected in stems of 10-wk-old Mo17 and Mo17^{ms39}. The analysis demonstrated the downregulation of seven YUC family genes in Mo17^{ms39} stem (Fig. 8-D). Additionally, six AUXIN/INDOLE ACETIC ACID (Aux/IAA) family genes involved in IAA signaling (Casanova-Sáez *et al*. 2021), were selected and detected in stems of 10-wk-old Mo17 and Mo17^{ms39}. The analysis revealed the downregulation of five Aux/IAA family genes in Mo17^{ms39} stem (Fig. 8-D). These results indicate that the mutation of *ZmCals12* inhibits IAA biosynthesis and signaling.

4. Discussion

4.1. Pleiotropic phenotype of the *Zmcals12* mutants is related to the reduced sugar transport

The mutation of *ZmCals12* results in plant dwarfing and male sterility (Appendix F) (Niu *et al*. 2023). These phenotypic manifestations align with previously characterized carbohydrate partitioning-defect mutants, including *Cpd1*, *cpd28*, *cpd33*, *cpd47*, *chl3*, *sut1*, and *sweet13a;b;c* (Baker *et al.* 2016; Bezrutczyk *et al.* 2018; Julius *et al.* 2018; Tran *et al*. 2019; Julius *et al*. 2021; Qin *et al*. 2022). These mutants exhibit impairments in phloem loading and/or sucrose transport to sink tissues. In our study, *in situ* staining experiments revealed that excessive starch accumulation was observed in the BS cells of *Zmcals12* mutants (Fig. 5-A). TEM revealed excessive starch accumulation in the BS chloroplasts of Mo17^{ms39} mature leaf (Fig. 5-C). Moreover, analysis of starch and soluble sugar contents demonstrated irregular distribution patterns in various tissues of Mo17^{ms39} compared to Mo17 (Figs. 5-B and 6). These findings indicate that the mutation of *ZmCals12* impairs sugar transport from source leaves to sink tissues, thereby reducing energy availability for plant growth and development.

In addition, previous research has established that elevated soluble sugar levels inhibit photosynthetic efficiency (Aguilera-Alvarado and Sanchez-Nieto 2017; Qin *et al.* 2022). This study demonstrates that excessive carbohydrate

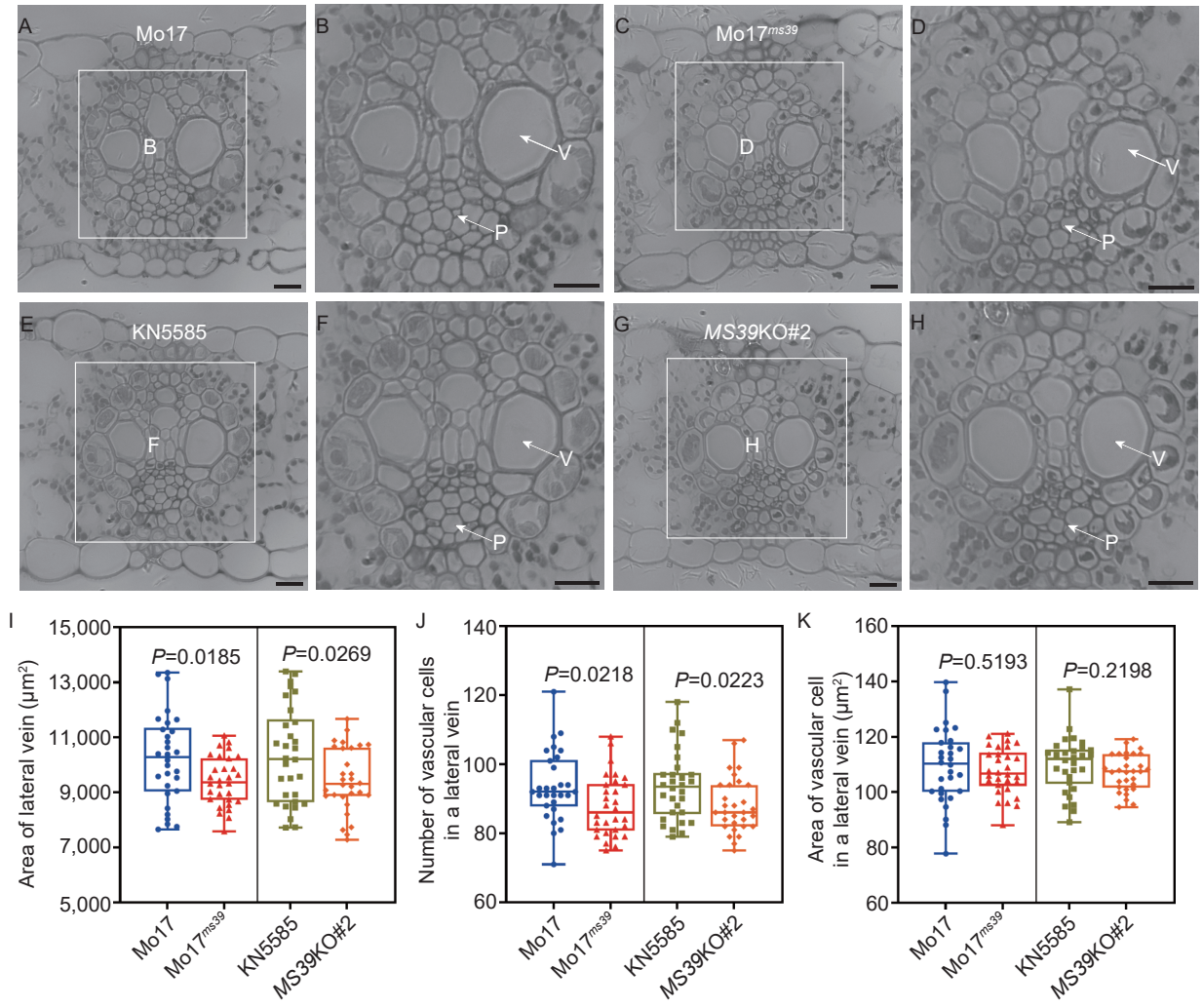


Fig. 7 Observation and comparison of leaf veins. A–H, paraffin sections of lateral veins from 5-wk-old Mo17, Mo17^{ms39}, KN5585 and *MS39*KO#2 mature leaves. V, xylem vessel; P, phloem. Scale bars=20 μm. I–K, statistical analysis of the lateral vein area, vascular cells (VCs) number, and VC area in 5-wk-old Mo17, Mo17^{ms39}, KN5585 and *MS39*KO#2 mature leaves (*n*=30 lateral veins). The central line, box and whiskers in boxplots indicate the median, the first and third quartiles, and the minimum and maximum values, respectively. Statistical significance was determined using a two-tailed Student's *t*-test.

accumulation in *ms39* source leaf results in increased osmium globules and chloroplast membrane disruption (Fig. 5-C). These observations suggest that excessive carbohydrate accumulation in *ms39* leaf diminishes photosynthetic efficiency.

4.2. ZmCals12 is involved in callose deposition and regulates symplastic transport

Sugar transport in plants includes both symplastic and apoplastic routes, which are mediated by PDs and sugar transporter proteins, respectively (Slewinski and Braun 2010; Braun *et al*. 2014; Yadav *et al*. 2015; Julius *et al*. 2017). PD permeability is regulated by PD-associated proteins and callose deposition/degradation at the PD neck (Thomas *et al*. 2008; Lee *et al*. 2011; Han *et al*. 2014; Kitagawa and Jackson 2017; Wu *et al*. 2018). In our study, histochemical GUS activity assay and mRNA ISH revealed that *ZmCals12* is mainly expressed in the vascular transport system (Fig. 1). Callose immunofluorescence localization demonstrated that ZmCals12 loss-of-function reduces callose deposition in PDs and around PCs of vascular bundle, attributable to decreased callose synthase activity (Fig. 2; Appendix C). Moreover, DANS assay indicated reduced PD permeability in photosynthetic cells and diminished transport competence in leaf veins of *Zmcals12* mutants (Figs. 3 and 4). These results demonstrate that normal symplastic transport requires ZmCals12-mediated callose deposition in maize.

It's worth noting that the reduced symplastic transport in the *Zmcals12* mutants is accompanied by decreased callose deposition, which seems to be a counter-intuitive finding. While excessive callose deposition can restrict PD permeability, and reduced callose levels can enhance PD permeability (Benitez-Alfonso *et al.* 2013), evidence suggests that moderate callose deposition is essential for proper symplastic transport (Barratt *et al.* 2011; Xie *et al.* 2011; Shi *et al.* 2015; Song *et al.* 2016). Furthermore, callose equilibration in PD serves a crucial function in regulating size exclusion limit (SEL) and symplastic transport (De Storme and Geelen 2014). Therefore, we think that decreased callose deposition in the *Zmcals12* mutants likely disrupts the callose equilibration in PDs, thereby limiting symplastic

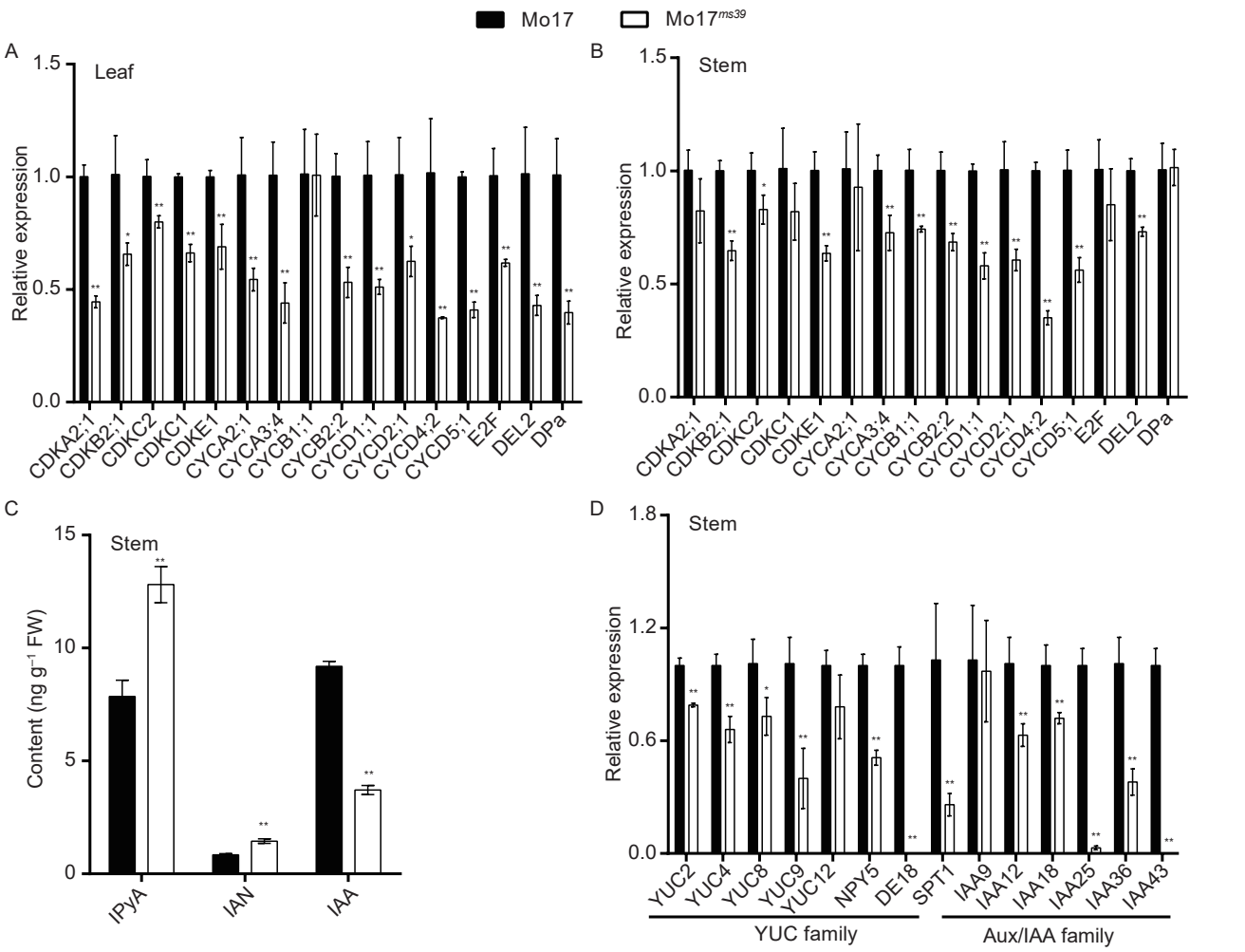


Fig. 8 RT-qPCR analysis of cell cycle-related genes (CCRs), YUCCA (YUC) and AUXIN/INDOLE ACETIC ACID (Aux/IAA) family genes, and quantification of auxin (IAA) biosynthetic components. A and B, expression levels of CCRs in 5-wk-old mature leaves and 10-wk-old stems of Mo17 and Mo17^{ms39}. C, contents of IAA biosynthesis components in stems of 10-wk-old Mo17 and Mo17^{ms39}. D, expression levels of YUC and Aux/IAA family genes in stems of 10-wk-old Mo17 and Mo17^{ms39}. Data are mean±SD (n=3). Asterisks indicate significant differences determined using a two-tailed Student's t-test (*, P<0.05; **, P<0.01).

transport. In addition, modifications in PD frequency or structure can influence symplastic transport (Russin *et al.* 1996; Provencher *et al*. 2001; Xu *et al*. 2012; Han *et al.* 2014). In our study, callose immunofluorescence localization revealed reduced fluorescence in PDs of the *Zmcals12* mutants, suggesting that the mutation of *ZmCals12* may impede PD formation and decrease PD numbers. Additional research is required to validate this hypothesis.

4.3. ZmCals12 affects sugar transport by regulating the development of VCs

Callose synthase genes also participate in regulating vascular bundle development, as exemplified by *OsSEM1*, *ZmTDY2* and *ZmSLM1*, which are expressed in leaf vascular tissue and are essential for plant growth and development (Slewinski *et al.* 2012; Wang *et al*. 2022; Zhong *et al*. 2023). The *ZmTDY2* mutation results in incomplete vascular bundle differentiation (Slewinski *et al*. 2012). The *ZmSLM1* mutation leads to vascular bundle development defects (Zhong *et al*. 2023), and the *OsSEM1* mutation diminishes the area and number of VCs (Wang *et al*. 2022). Our research verified that the mutation of *ZmCals12* results in less-developed VCs (Fig. 7). These results demonstrate the significant role of callose synthase genes in maintaining normal vascular bundle development. Beyond callose synthase genes, previous research has shown that *CPD1* and *Bk2L3* also influence maize vascular bundle structure (Julius *et al*. 2018). *Bk2L3* participates in cell wall development, and its loss-of-function affects the ultrastructure of SE cell walls and carbohydrate partitioning (Julius *et al*. 2021). These results indicate that the normal development of vascular tissue is important for sugar transport.

Loss-of-function of OsSEM1 impacts VC development through suppression of cell cycle-related gene expression (Wang *et al*. 2022). Our research revealed decreased expression levels of cell cycle-related genes in Mo17^{ms39} leaf and stem compared to Mo17 (Fig. 8-A and B). These genes function in cell cycle progression, including the transitions between G1/S and G2/M phases, and DNA replication during S phase (Del *et al.* 2002; Vandepoele *et al.* 2002; Dewitte and Murray 2003; Shimotohno *et al.* 2004; Menges

et al. 2005; Inzé and De Veylder 2006). These results indicate that *ZmCals12* affects leaf vein and internode development through cell cycle progression inhibition. The precise mechanism by which *ZmCals12* regulates cell cycle progression requires further investigation.

4.4. ZmCals12-mediated sugar transport impacts plant height development by regulating IAA biosynthesis and signaling

In our study, mRNA ISH analysis revealed that ZmCals12 was not expressed in elongating internode (Fig. 1-B), suggesting that *ZmCals12* may indirectly regulate internode development. Our research demonstrated that loss-of-function of ZmCals12 reduced sugar transport to stem (Fig. 6). This raises the question of how reduced sugar transport affects internode development. Previous studies have shown that sugar functions as a signaling molecule influencing endosperm cell differentiation and development (Liao *et al*. 2020). In maize, sugars also regulate cell fate in the BETL *via* cross-talk with IAA, where altered sugar levels and decreased IAA levels reduce cell wall ingrowths in the BETL of maize mutant *mn1* (Chourey et al. 2010). Our research found significantly lower IAA content in Mo17^{ms39} stem compared to Mo17 (Fig. 8-C). Additionally, the expression levels of YUCs, which convert IPyA to IAA, were down-regulated in Mo17^{ms39} leaf and stem (Fig. 8-D). The IPyA pathway represents the primary route for IAA synthesis in plants (Casanova-Sáez et al. 2021). Thus, the mutation of *ZmCals12* reduced IAA biosynthesis through inhibition of the IPyA pathway. Furthermore, the expression levels of IAAs, involved in IAA signaling, were also down-regulated in Mo17^{ms39} leaf and stem (Fig. 8-D). These findings indicate that ZmCals12-mediated sugar transport impacts plant height development by regulating IAA biosynthesis and signaling.

5. Conclusion

This study demonstrates that ZmCals12 impacts maize growth and development by regulating symplastic transport. Loss-of-function of ZmCals12 results in decreased PD permeability and less-developed VCs, reducing sugar transport from source leaves to sink tissues, hindering the development of internode and male flower, and thus resulting in plant dwarfing and tassel abortion.

Acknowledgements

This study was supported by grants from the National Natural Science Foundation of China (31771876), the Biological Breeding Program of State Key Laboratory of Sichuan Agricultural University, China (SKL-ZY202234) and the Sichuan Province Science and Technology Program, China (2021YFYZ0011 and 2021YFYZ0017).

Declaration of competing interest

The authors declare that they have no conflict of interest.

Declaration of generative AI and AI-assisted technologies in the writing process

The authors declare that they did not use AI in the preparation and writing of this manuscript.

Appendices associated with this paper are available at https://doi.org/10.1016/j.jia.2024.05.010

References

Aguilera-Alvarado G P, Sanchez-Nieto S. 2017. Plant hexokinases are multifaceted proteins. *Plant and Cell Physiology*, **58**, 1151–1160.

Amsbury S, Kirk P, Benitez-Alfonso Y. 2017. Emerging models on the regulation of intercellular transport by plasmodesmata-associated callose. *Journal of Experimental Botany*, **69**, 105–115.

Baker R F, Braun D M. 2007. *Tie-dyed1* functions non-cell autonomously to control carbohydrate accumulation in maize leaves. *Plant Physiology*, **144**, 867–878.

Baker R F, Braun D M. 2008. *Tie-dyed2* functions with *Tie-dyed1* to promote carbohydrate export from maize leaves. *Plant Physiology*, **146**, 1085–1097.

Baker R F, Leach K A, Boyer N R, Swyers M J, Benitez-Alfonso Y, Skopelitis T, Luo A, Sylvester A, Jackson D, Braun D M. 2016. Sucrose transporter *ZmSut1* expression and localization uncover new insights into sucrose phloem loading. *Plant Physiology*, **172**, 1876–1898.

Baker R F, Slewinski T L, Braun D M. 2013. The *tie-dyed* pathway promotes symplastic trafficking in the phloem. *Plant Signaling and Behavior*, **8**, e24540.

Barratt D H, Kölling K, Graf A, Pike M, Calder G, Findlay K, Zeeman S C, Smith A M. 2011. Callose synthase GSL7 is necessary for normal phloem transport and inflorescence growth in *Arabidopsis*. *Plant Physiology*, **155**, 328–341.

van Bel A J, Knoblauch M. 2000. Sieve element and companion cell: The story of the comatose patient and the hyperactive nurse. *Functional Plant Biology*, **27**, 477–487.

Benitez-Alfonso Y, Faulkner C, Pendle A, Miyashima S, Helariutta Y, Maule A. 2013. Symplastic intercellular connectivity regulates lateral root patterning. *Developmental Cell*, **26**, 136–147.

Bezrutczyk M, Hartwig T, Horschman M, Char S N, Yang J, Yang B, Frommer W B, Sosso D. 2018. Impaired phloem loading in *zmsweet13a*,*b*,*c* sucrose transporter triple knock-out mutants in *Zea mays*. *New Phytologist*, **218**, 594–603.

Bezrutczyk M, Zöllner N R, Kruse C P S, Hartwig T, Lautwein T, Köhrer K, Frommer W B, Kim J Y. 2021. Evidence for phloem loading *via* the abaxial bundle sheath cells in maize leaves. *The Plant Cell*, **33**, 531–547.

Botha C E J, Cross R H M, van Bel A J E, Peter C I. 2000. Phloem loading in the sucrose-export-defective (*SXD-1*) mutant maize is limited by callose deposition at plasmodesmata in bundle sheath-vascular parenchyma interface. *Protoplasma*, **214**, 65–72.

Braun D M, Slewinski T L. 2009. Genetic control of carbon partitioning in grasses: Roles of *Sucrose Transporters* and *Tie-dyed* loci in phloem loading. *Plant Physiology*, **149**, 71–81.

Braun D M, Wang L, Ruan Y L. 2014. Understanding and manipulating sucrose phloem loading, unloading, metabolism, and signalling to enhance crop yield and food security. *Journal of Experimental Botany*, **65**, 1713–1735.

Casanova-Sáez R, Mateo-Bonmatí E, Ljung K. 2021. Auxin metabolism in plants. *Cold Spring Harbor Perspectives in Biology*, **13**, a039867.

Chen X Y, Zhang H, Sun H Y, Luo H B, Zhao L, Dong Z B, Yan S S, Zhao C, Liu R Y, Xu C Y, Li S, Chen H B, Jin W W. 2017. *IRREGULAR POLLEN EXINE1* is a novel factor in anther cuticle and pollen exine formation. *Plant Physiology*, **173**, 307–325.

Chourey P S, Li Q B, Kumar D. 2010. Sugar-hormone cross-talk in seed development: Two redundant pathways of IAA biosynthesis are regulated differentially in the invertase-deficient *miniature1* (*mn1*) seed mutant in maize. *Molecular Plant*, **3**, 1026–1036.

Cui W, Lee J Y. 2016. *Arabidopsis* callose synthases CalS1/8 regulate plasmodesmal permeability during stress. *Nature Plants*, **2**, 16034.

Del P J, Boniotti M B, Gutierrez C. 2002. *Arabidopsis* E2Fc functions in cell division and is degraded by the ubiquitin-SCF(AtSKP2) pathway in response to light. *The Plant Cell*, **14**, 3057–3071.

Dewitte W, Murray J A. 2003. The plant cell cycle. *Annual Review of Plant Biology*, **54**, 235–264.

Eom J S, Chen L Q, Sosso D, Julius B T, Lin I W, Qu X Q, Braun D M, Frommer W B. 2015. SWEETs, transporters for intracellular and intercellular sugar translocation. *Current Opinion in Plant Biology*, **25**, 53–62.

Esau K. 1977. *Anatomy of Seed Plants*. John Wiley and Sons, New York.
Evert R F. 1982. Sieve-tube structure in relation to function. *Bioscience*, **32**, 789–795.
Evert R F, Eschrich W, Heyser W. 1978. Leaf structure in relation to solute transport and phloem loading in *Zea mays* L. *Planta*, **138**, 279–294.
Gallei M, Luschnig C, Friml J. 2020. Auxin signalling in growth: Schrödinger's cat out of the bag. *Current Opinion in Plant Biology*, **53**, 43–49.
Han X, Hyun T K, Zhang M, Kumar R, Koh E J, Kang B H, Lucas W J, Kim J Y. 2014. Auxin-callose-mediated plasmodesmal gating is essential for tropic auxin gradient formation and signaling. *Developmental Cell*, **28**, 132–146.
Hu X, Cheng X, Jiang H, Zhu S, Cheng B, Xiang Y. 2010. Genome-wide analysis of cyclins in maize (*Zea mays*). *Genetics and Molecular Research*, **9**, 1490–1503.
Inzé D, De Veylder L. 2006. Cell cycle regulation in plant development. *Annual Review of Genetics*, **40**, 77–105.
Julius B T, Leach K A, Tran T M, Mertz R A, Braun D M. 2017. Sugar transporters in plants: New insights and discoveries. *Plant and Cell Physiology*, **58**, 1442–1460.
Julius B T, McCubbin T J, Mertz R A, Baert N, Knoblauch J, Grant D G, Conner K, Bihmidine S, Chomet P, Wagner R, Woessner J, Grote K, Peevers J, Slewinski T L, McCann M C, Carpita N C, Knoblauch M, Braun D M. 2021. Maize *Brittle Stalk2-Like3*, encoding a COBRA protein, functions in cell wall formation and carbohydrate partitioning. *The Plant Cell*, **33**, 3348–3366.
Julius B T, Slewinski T L, Baker R F, Tzin V, Zhou S, Bihmidine S, Jander G, Braun D M. 2018. Maize *Carbohydrate partitioning defective1* impacts carbohydrate distribution, callose accumulation, and phloem function. *Journal of Experimental Botany*, **69**, 3917–3931.
Kamal K Y, Khodaeiaminjan M, Yahya G, El-Tantawy A A, Abdel El-Moneim D, El-Esawi M A, Abd-Elaziz M A A, Nassrallah A A. 2021. Modulation of cell cycle progression and chromatin dynamic as tolerance mechanisms to salinity and drought stress in maize. *Physiologia Plantarum*, **172**, 684–695.
Kitagawa M, Jackson D. 2017. Plasmodesmata-mediated cell-to-cell communication in the shoot apical meristem: How stem cells talk. *Plants* (Basel), **6**, 12.
Korasick D A, Enders T A, Strader L C. 2013. Auxin biosynthesis and storage forms. *Journal of Experimental Botany*, **64**, 2541–2555.
Lalonde S, Tegeder M, Throne-Holst M, Frommer W B, Patrick J W. 2003. Phloem loading and unloading of sugars and amino acids. *Plant Cell*, *and Environment*, **26**, 37–56.
Leach K A, Braun D M. 2016. Soluble sugar and starch extraction and quantification from maize (*Zea mays*) leaves. *Current Protocols in Plant Biology*, **1**, 139–161.
Leach K A, Tran T M, Slewinski T L, Meeley R B, Braun D M. 2017. *Sucrose transporter2* contributes to maize growth, development, and crop yield. *Journal of Integrative Plant Biology*, **59**, 390–408.
Lee J Y, Wang X, Cui W, Sager R, Modla S, Czymmek K, Zybaliov B, van Wijk K, Zhang C, Lu H, Lakshmanan V. 2011. A plasmodesmata-localized protein mediates crosstalk between cell-to-cell communication and innate immunity in *Arabidopsis*. *The Plant Cell*, **23**, 3353–3373.
Liao S, Wang L, Li J, Ruan Y L. 2020. Cell wall invertase is essential for ovule development through sugar signaling rather than provision of carbon nutrients. *Plant Physiology*, **183**, 1126–1144.
Liu H, Li X, Xiao J, Wang S. 2012. A convenient method for simultaneous quantification of multiple phytohormones and metabolites: Application in study of rice–bacterium interaction. *Plant Methods*, **8**, 2.
Liu M Y, Peng D L, Su W, Xiang C, Jian J Z, Zhao J, Peng H, Liu S M, Kong L A, Dai L Y, Huang W K, Liu J. 2022. Potassium sulphate induces resistance of rice against the root-knot nematode *Meloidogyne graminicola*. *Journal of Integrative Agriculture*, **21**, 3263–3277.
Livak K J, Schmittgen T D. 2001. Analysis of relative gene expression data using real-time quantitative PCR and the $2^{-\Delta\Delta CT}$ method. *Methods*, **25**, 402–408.
Ma Y, Baker R F, Magallanes-Lundback M, DellaPenna D, Braun D M. 2008. *Tie-dyed1* and *sucrose export defective1* act independently to promote carbohydrate export from maize leaves. *Planta*, **227**, 527–538.
Ma Y, Slewinski T L, Baker R F, Braun D M. 2009. *Tie-dyed1* encodes a novel, phloem-expressed transmembrane protein that functions in carbohydrate partitioning. *Plant Physiology*, **149**, 181–194.
Menges M, de Jager S M, Gruissem W, Murray J A. 2005. Global analysis of the core cell cycle regulators of Arabidopsis identifies novel genes, reveals multiple and highly specific profiles of expression and provides a coherent model for plant cell cycle control. *The Plant Journal*, **41**, 546–566.
Niu Q K, Shi Z W, Zhang P, Su S, Jiang B, Liu X W, Zhao Z F, Zhang S Z, Huang Q, Li C, Yu T, Yi H Y, Rong T Z, Cao M J. 2023. ZmMS39 encodes a callose synthase essential for male fertility in maize (*Zea mays* L.). *The Crop Journal*, **11**, 394–404.
Provencher L M, Miao L, Sinha N, Lucas W J. 2001. *Sucrose export defective1* encodes a novel protein implicated in chloroplast-to-nucleus signaling. *The Plant Cell*, **13**, 1127–1141.
Qin Y, Xiao Z Y, Zhao H L, Wang J, Wang Y R, Qiu F Z. 2022. *Starch phosphorylase 2* is essential for cellular carbohydrate partitioning in maize. *Journal of Integrative Plant Biology*, **64**, 1755–1769.
Roberts A G, Oparka K J. 2003. Plasmodesmata and the control of symplastic transport. *Plant Cell*, *and Environment*, **26**, 103–124.
Russin W A, Evert R F, Vanderveer P J, Sharkey T D, Briggs S P. 1996. Modification of a specific class of plasmodesmata and loss of sucrose export ability in the *sucrose export defective1* maize mutant. *The Plant Cell*, **8**, 645–658.
Shi X, Sun X, Zhang Z, Feng D, Zhang Q, Han L, Wu J, Lu T. 2015. GLUCAN SYNTHASE-LIKE 5 (GSL5) plays an essential role in male fertility by regulating callose metabolism during microsporogenesis in rice. *Plant and Cell Physiology*, **56**, 497–509.
Shi X, Wu J X, Zhou H T, Yang X H, Li T L, Zhang X J, Yang C, Han X. 2016. Defective callose walls and cell plates during abnormal meiosis cause male-sterility in the oat mutant *zbs1*. *Journal of Integrative Agriculture*, **15**, 241–248.
Shimotohno A, Umeda-Hara C, Bisova K, Uchimiya H, Umeda M. 2004. The plant-specific kinase CDKF;1 is involved in activating phosphorylation of cyclin-dependent kinase-activating kinases in *Arabidopsis*. *The Plant Cell*, **16**, 2954–2966.
Slewinski T L, Baker R F, Stubert A, Braun D M. 2012. *Tie-dyed2* encodes a callose synthase that functions in vein development and affects symplastic trafficking within the phloem of maize leaves. *Plant Physiology*, **160**, 1540–1550.
Slewinski T L, Braun D M. 2010. Current perspectives on the regulation of whole-plant carbohydrate partitioning. *Plant Science*, **178**, 341–349.
Slewinski T L, Garg A, Johal G S, Braun D M. 2010. Maize SUT1 functions in phloem loading. *Plant Signaling and Behavior*, **5**, 687–690.
Slewinski T L, Ma Y, Baker R F, Huang M, Meeley R, Braun D M. 2008. Determining the role of *Tie-dyed1* in starch metabolism: Epistasis analysis with a maize ADP-glucose pyrophosphorylase mutant lacking leaf starch. *Journal of Heredity*, **99**, 661–666.
Slewinski T L, Meeley R, Braun D M. 2009. *Sucrose transporter1* functions in phloem loading in maize leaves. *Journal of Experimental Botany*, **60**, 881–892.
Song L Z, Wang R C, Zhang L, Wang Y M, Yao S G. 2016. *CRR1* encoding callose synthase functions in ovary expansion by affecting vascular cell patterning in rice. *The Plant Journal*, **88**, 620–632.
Sosso D, Luo D, Li Q B, Sasse J, Yang J, Gendrot G, Suzuki M, Koch K E, McCarty D R, Chourey P S, Rogowsky P M, Ross-Ibarra J, Yang B, Frommer W B. 2015. Seed filling in domesticated maize and rice depends on SWEET-mediated hexose transport. *Nature Genetics*, **47**, 1489–1493.
De Storme N, Geelen D. 2014. Callose homeostasis at plasmodesmata: Molecular regulators and developmental relevance. *Frontiers in Plant Science*, **5**, 138.
Thomas C L, Bayer E M, Ritzenthaler C, Fernandez-Calvino L, Maule A J. 2008. Specific targeting of a plasmodesmal protein affecting cell-to-cell communication. *PLoS Biology*, **6**, e7.
Tran T M, McCubbin T J, Bihmidine S, Julius B T, Baker R F, Schauflinger M, Weil C, Springer N, Chomet P, Wagner R, Woessner J, Grote K, Peevers J, Slewinski T L, Braun D M. 2019. Maize *Carbohydrate Partitioning Defective33* encodes an MCTP protein and functions in sucrose export from leaves. *Molecular Plant*, **12**, 1278–1293.
Vandepoele K, Raes J, De Veylder L, Rouzé P, Rombauts S, Inzé D. 2002. Genome-wide analysis of core cell cycle genes in

Arabidopsis. *The Plant Cell*, **14**, 903–916.
Vatén A, Dettmer J, Wu S, Stierhof Y D, Miyashima S, Yadav S R, Roberts C J, Campilho A, Bulone V, Lichtenberger R, Lehesranta S, Mähönen A P, Kim J Y, Jokitalo E, Sauer N, Scheres B, Nakajima K, Carlsbecker A, Gallagher K L, Helariutta Y. 2011. Callose biosynthesis regulates symplastic trafficking during root development. *Developmental Cell*, **21**, 1144–1155.
Verma D P, Hong Z. 2001. Plant callose synthase complexes. *Plant Molecular Biology*, **47**, 693–701.
Wang Y, Sun J, Deng C, Teng S, Chen G, Chen Z, Cui X, Brutnell T P, Han X, Zhang Z, Lu T. 2022. Plasma membrane-localized SEM1 protein mediates sugar movement to sink rice tissues. *The Plant Journal*, **109**, 523–540.
Wang Z, Wei K, Xiong M, Wang J D, Zhang C Q, Fan X L, Huang L C, Zhao D S, Liu Q Q, Li Q F. 2021. Glucan, Water-Dikinase 1 (GWD1), an ideal biotechnological target for potential improving yield and quality in rice. *Plant Biotechnology Journal*, **19**, 2606–2618.
Wu S W, Kumar R, Iswanto A, Kim J Y. 2018. Callose balancing at plasmodesmata. *Journal of Experimental Botany*, **69**, 5325–5339.
Xie B, Wang X M, Zhu M S, Zhang Z M, Hong Z L. 2011. *CalS7* encodes a callose synthase responsible for callose deposition in the phloem. *The Plant Journal*, **65**, 1–14.
Xu M, Cho E, Burch-Smith T M, Zambryski P C. 2012. Plasmodesmata formation and cell-to-cell transport are reduced in *decreased size exclusion limit 1* during embryogenesis in *Arabidopsis*. *Proceedings of the National Academy of Sciences of the United States of America*, **109**, 5098–5103.
Yadav U P, Ayre B G, Bush D R. 2015. Transgenic approaches to altering carbon and nitrogen partitioning in whole plants: Assessing the potential to improve crop yields and nutritional quality. *Frontiers in Plant Science*, **6**, 275.
Yang B, Wang J, Yu M, Zhang M, Zhong Y, Wang T, Liu P, Song W, Zhao H, Fastner A, Suter M, Rentsch D, Ludewig U, Jin W, Geiger D, Hedrich R, Braun D M, Koch K E, McCarty D R, Wu W H, *et al.* 2022. The sugar transporter ZmSUGCAR1 of the nitrate transporter 1/peptide transporter family is critical for maize grain filling. *The Plant Cell*, **34**, 4232–4254.
Zambryski P, Crawford K. 2000. Plasmodesmata: Gatekeepers for cell-to-cell transport of developmental signals in plants. *Annual Review of Cell and Developmental Biology*, **16**, 393–421.
Zhao Y. 2018. Essential roles of local auxin biosynthesis in plant development and in adaptation to environmental changes. *Annual Review of Plant Biology*, **69**, 417–435.
Zhong W S, Zheng C, Dong L, Kang L, Yang F. 2023. The maize callose synthase *SLM1* is critical for a normal growth by controlling the vascular development. *Molecular Breeding*, **43**, 2.
Zhu Y H, Shi Z W, Li S Z, Liu H Y, Liu F X, Niu Q K, Li C, Wang J, Rong T Z, Yi H Y, Cao M J. 2018. Fine mapping of the novel male-sterile mutant gene *ms39* in maize originated from outer space flight. *Molecular Breeding*, **38**, 125.

Executive Editor-in-Chief Xueyong Zhang
Managing Editor Ning Wang